JTTEE5 19:1255–1266
DOI: 10.1007/s11666-010-9527-7
1059-9630/$19.00 © ASM International

Evaluation of Parameters for Assessment of Inter-Splat Bond Strength in Cold-Sprayed Coatings

G. Sundararajan, Naveen M. Chavan, G. Sivakumar, and P. Sudharshan Phani

(Submitted September 18, 2009; in revised form April 28, 2010)

The quality and performance of cold spray coatings are largely determined by the extent and strength of bonding between the adjacent splats. Usually, the extent of inter-splat bonding is only qualitatively estimated by examining the polished and etched sectioned surfaces of the coated sample. Thus, there is a clear need for indirect techniques to quantitatively estimate the extent of inter-splat bonding so that they can serve as quality control tools. In this study, elastic modulus, electrical conductivity, and critical load for inter-splat debonding as determined using a scratch test are considered as possible parameters for the estimation of the extent of inter-splat bonding using four different cold spray coatings (Ag, Cu, 316 Stainless Steel, and Zn) as model coatings. It is demonstrated that all the three parameters are capable of quantifying the extent of inter-splat bonding.

Keywords cold spray coating, critical load for inter-splat debonding, elastic modulus, electrical conductivity, inter-splat bond strength

1. Introduction

Cold spray coatings, belonging to the family of thermal spray coatings, are formed through repeated impacts of powder particles onto the substrate at high velocities (500-1200 m/s), and as a result, exhibit very low porosities. Since the powder particles are heated only to maximum temperature of 500-600 °C in the cold spray technique, the composition and phases present in the powder feedstock are essentially retained in the final coating formed. In particular, the oxidation of powder particles during their flight (prior to impact onto the substrate) is minimal leading to near-zero oxide content in the coating with the attendant advantages like high electrical and thermal conductivity in the coating.

Cold spray coatings with attractive properties have been obtained in the case of pure metals such as Cu, Al, Ti, Ni, Fe, and Ta (Ref 1-9) and also in the case of metallic alloys such as stainless steels, Inconel, Ni-Cr alloys, Ti-6Al-4V, and steels (Ref 10-17). In all these coatings, the coating property and its performance are substantially influenced by the extent of bonding between the splats (powder particles which flatten on impacting the substrate are defined as splats) that make up the coating. It is believed that the bonding between the splats is essentially the result of high pressure generated in the contact surface, which helps in breaking and pinching out the oxide layer on splat surfaces in contact and thus enhancing the bonding, and also adiabatic shearing effects which concentrate the deformation on impact to the contact region causing a substantial temperature rise in the contact area, which again aids bonding (Ref 18-24).

Inspite of the fact that the above two factors aid inter-splat bonding, in a typical cold spray coating, only a fraction of the splats are well bonded with the neighboring splats. Further, the fraction of well bonded splats depend on the material being coated and on the coating process parameters. The fraction of the well-bonded splats in a cold spray coating can be qualitatively estimated by etching the sectioned and polished cold spray-coated sample and then observing the surface in an optical or scanning electron microscope. Etching usually opens up the poorly bonded inter-splat boundaries and, thus, the proportion of the opened-up boundaries is an indication of the fraction of poorly bonded boundaries. However, the above technique is subjective and tedious and not amenable to quantification. Thus, it makes sense to develop indirect methods which measure parameters/properties which are strongly influenced by the proportion of inter-splat boundaries which are well bonded and also by the strength of the bond in the case of well-bonded splats.

A perusal of the literature in this regard and also our own study indicates that the elastic modulus and the electrical conductivity of the thermal spray coatings are strongly influenced by the nature and the extent of bonding between the splats. In addition, it is also felt that scratch testing wherein a diamond stylus is pressed against the surface of a thick coating (e.g. cold spray coating) with continuous increase in the load is also capable of providing information on inter-splat bonding. Scratch test has already been well established for thin coatings, wherein it is able to evaluate the coating-substrate adhesion/bond

G. Sundararajan, Naveen M. Chavan, G. Sivakumar, and **P. Sudharshan Phani**, International Advanced Research Centre for Powder Metallurgy and New Materials, Hyderabad, India. Contact e-mail: gsundar@arci.res.in.

strength in terms of the critical load at which the coating delaminates (Ref 25). In the case of thick coatings; scratch testing actually evaluates the critical load for inter-splat debonding as will be demonstrated in this article.

The objective of this study is thus to assess and demonstrate the usefulness of elastic modulus, electrical conductivity, and critical load for inter-splat debonding as parameters capable of quantifying the extent and strength of the inter-splat bonding in the case of cold spray coatings. Toward the above purpose, coatings of Zn, Ag, Cu, and SS 316L have been deposited on mild steel substrate using the cold spray technique, and further these coatings have been heat treated at various temperatures to improve the inter-splat bonding. The elastic modulus, electrical conductivity, and critical load for splat debonding have been evaluated for all the above coatings in the as-coated and heat-treated conditions. It is further shown that all these parameters appear to correlate well with each other and also with the extent of inter-splat bonding as observed independently through SEM micrographs of sectioned and polished surfaces of the cold spray coatings.

2. Experimental Details

2.1 Cold Spray Coatings and Heat Treatment

All the coatings were deposited using the in-house facility for cold spraying. A De Laval nozzle with a rectangular exit was used and compressed air was used as both the process and powder carrier gas. Commercially available powders of silver, zinc, copper (Innomet, India), and SS 316L (Prax Air, USA) were used as the feedstock. The silver, copper, and SS 316L powders were manufactured by air atomization, whereas the Zn powders were produced by water atomization. Figure 1 illustrates the morphology of all the four powders used in this study, and it is clear that Zn powder is more flaky/angular compared to the other three powders which are bulky and more rounded. The measurement of powder particle size distribution of the four powders indicated their average sizes (i.e., diameter at 50%) to be in the range of 25-35 μm s. The Zn powder was also characterized for oxygen content on its surfaces (in the form of oxides) using x-ray photoelectron spectroscopy (XPS; Omicron, UK).

The four powders were chosen not only on the basis of their cold sprayability, but also because they represented a wide range with regard to the melting point, elastic modulus, and electrical conductivity as illustrated in Table 1. Thus, it was felt that the use of such divergent powders as feedstock for cold spraying will provide a more general validity for the use of various indirect parameters for assessing inter-splat bonding.

The mild steel samples were grit blasted and subjected to ultrasonic cleaning prior to the coating deposition. In order to optimize the cold spray coating process parameters for each powder, the stagnation pressure was varied over the range 10-20 bar and gas preheat temperature from 300 to 475 °C (Ref 26). In the case of silver, electrical conductivity of the coating was utilized to optimize the coating process parameter since deposition efficiency was good over a broad range of parameters. In the case of other three powders, deposition efficiency of the coating was considered while optimizing the process parameters.

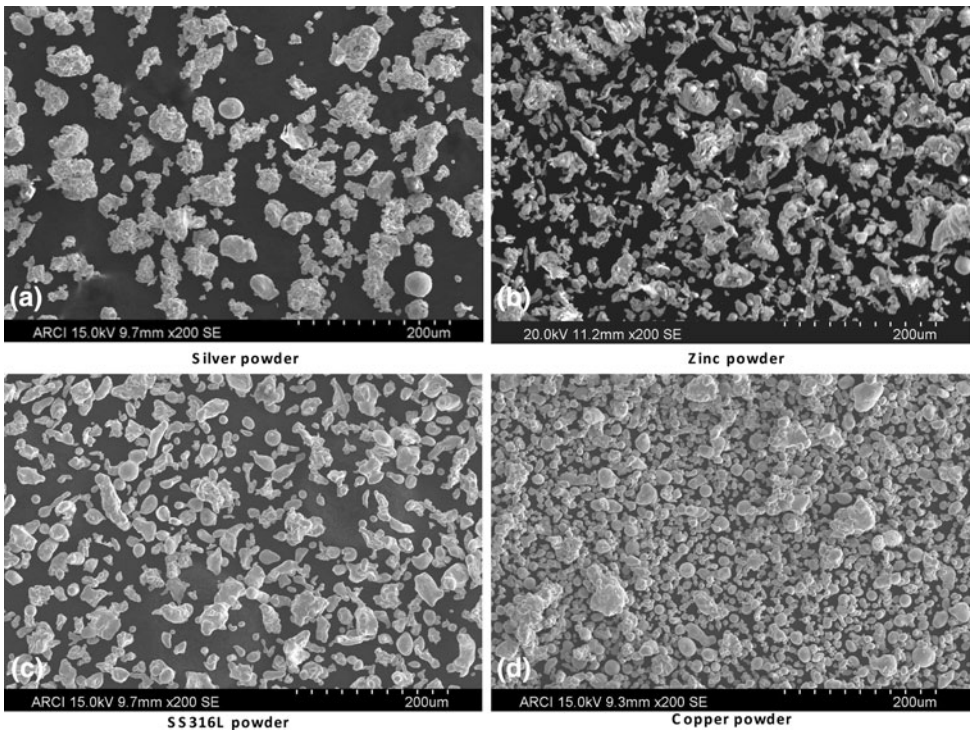

Fig. 1 SEM micrographs of the feedstock powders (a) Silver (b) Zinc (c) SS 316L, and (d) Copper

Table 1 The bulk material properties of Ag, Cu, Zn and SS 316L

Coating	Melting point, T_m, K (a)	Elastic modulus, E_b, GPa (a)	Electrical conductivity, σ_b, MS/m (a)
Ag	1233	83	63.00
Cu	1356	130	53.00
Zn	693	104	16.60
SS 316L	1623	193	1.35

(a) All data from Ref 36

Table 2 The optimized process parameters for the four cold spray coatings

Coating	Stagnation pressure, bar	Gas preheat temperature, °C	Stand off distance, mm	Powder feed rate, g/min
Silver	20	450	15	34.00
Copper	20	400	15	29.00
Zinc	20	350	15	23.10
SS 316L	20	475	15	26.00

Table 3 Details regarding the heat treatment of cold spray coatings

Coating	Heat treatment temperature, °C	Soaking time, h	Atmosphere
Silver	400	1	Argon
	400	1	Vacuum
Copper	600	1	Vacuum
	800	1	Vacuum
Zinc	350	10	Argon
	400	1	Air
SS 316L	800	1	Air
	1100	1	Air

Table 2 provides the optimized spray conditions for all the four coatings under study.

All the four coatings were heat treated at various temperatures to observe its effect on coating properties and in particular inter-splat bonding. The heat-treatment conditions are provided in Table 3. All the coatings were furnace cooled after the soaking period except those of SS 316L coatings which were air cooled.

2.2 Coating Characterization

The coated samples were sectioned and polished. They were then etched to observe the microstructure. An aqueous solution of two parts of 3% H_2O_2 + one part of NH_4OH + one part of distilled water was used to etch silver coatings. Zinc coatings were etched using a solution containing 100 g/L of NaOH in water, and the copper coatings were etched using a reagent containing 5 g $FeCl_3$, 10 mL HCl, and 100 mL H_2O. In the case of SS 316L, etching was not required to reveal the microstructure. The porosity of the coating was estimated on sectioned and polished surfaces using an image analyzer (Image ProPlus, Media Cybernetics, USA) in conjunction with the SEM prior to etching.

The hardness of the coatings were measured on polished and sectioned surface of the coating (without etching) using a Vickers microhardness tester (Leitz-112473, Germany) at a load of 200 g. At least 10 measurements were carried out on each sample, at random locations, to obtain the average value of the Vickers hardness (H_v). The associated scatter with average value of H_v was ±6%. The hardness values were obtained at room temperature on both as-coated and heat-treated samples. The elastic moduli of the coatings, in the as-coated and heat-treated conditions, was obtained using a nanoindentor (MTS System Corporation, USA) at 200 g load utilizing the technique described by Oliver and Pharr (Ref 27). The electrical conductivity of the coatings was measured using an eddy current-based coating conductivity gage (Sigma Test 2.069, Foerster, Germany). Measurements were taken at 10 different locations on the polished coated specimens, and the average value reported here had a scatter of ±10%.

The scratch tester (CSM Revetest, Switzerland) was utilized to get an estimate of the critical load (L_c) at which cracks started appearing at the base of the scratch formed on the coating surface. Scratch tests were performed on polished and unetched top surfaces of the Cu, Ag, Zn, and SS 316L coatings in the as-coated and also on coated and heat-treated samples (heat treated at 800 °C for Cu, 400 °C for Ag, 350 °C for Zn, and 1100 °C for SS 316L coatings). During the test, a Rockwell-type diamond spherical tip indentor with a radius of 100 μm was loaded against the coated sample and the load was progressively increased from 0.9 to 5 N at a loading rate of 6.5 N/min while the sample was moved at a speed of 10 mm/min. As a result, a scratch which progressively increases in width and depth was formed as schematically depicted in Fig. 2(a). The bottom of the scratch was then examined in the SEM as it progressively increased in width, i.e., along direction X in Fig. 2(a). First, a diamond paste was used to polish the coated surface prior to carrying out the scratch testing. However, in this case, the diamond polishing resulted in pullout of some of the splats and, therefore, it was difficult to distinguish cracks from the pullouts. In order to avoid these problems, colloidal silica was used as the polishing medium, and this resulted in polished coated surface free of pullouts; it was now possible to distinguish the cracking of the scratch bottom without any ambiguity. Initially and up to distances less than X_c (marked in Fig. 2a), the scratch bottom exhibited only splat boundaries decorated by pores as illustrated in the micrograph (Fig. 2b) taken from region 1 marked in Fig. 2(a). The region marked 2 in Fig. 2(a) represents the regions outside the scratch, and in this region also, only splat boundaries decorated by pores as illustrated in Fig. 2(c) were observed. Thus, for $X < X_c$, the microstructure of splat bottom was identical to that of the original coated surface. In contrast for distances greater than X_c (Fig. 2a), the scratch bottom indicated the presence of cracks formed by the joining of pre-existing pores under the influence of scratching stress. Since the pores were located along inter-splat boundaries, cracks also formed along the same

boundary. This is illustrated in the micrographs (Fig. 2d) taken from region 3 marked in Fig. 2(a). The regions outside the scratch (for $X > X_c$) were also examined, and this region (marked as 4 in Fig. 2a) did not exhibit any cracks but only splat boundaries decorated by pores as can be observed from Fig. 2(e). To complete the picture, a low magnification view of the scratch is presented in Fig. 2(f) and also a higher magnification view of the scratch beyond X_c (Fig. 2g). Once the critical distance X_c was determined as above, the load applied corresponding to the above critical distance (X_c) was estimated from the Load-Displacement curve recorded by scratch tester (Fig. 2h), and this load was defined as the critical load (L_c) for inter-splat debonding at the base of the scratch. The error in determining the value of L_c was approximately ±5% for L_c values greater than 1.5 N and about ±10% for L_c values lower than 1.5 N. In our opinion, L_c determined as above, should be a good measure of the inter-splat bond strength and thus L_c is henceforth referred to as the critical load for inter-splat debonding.

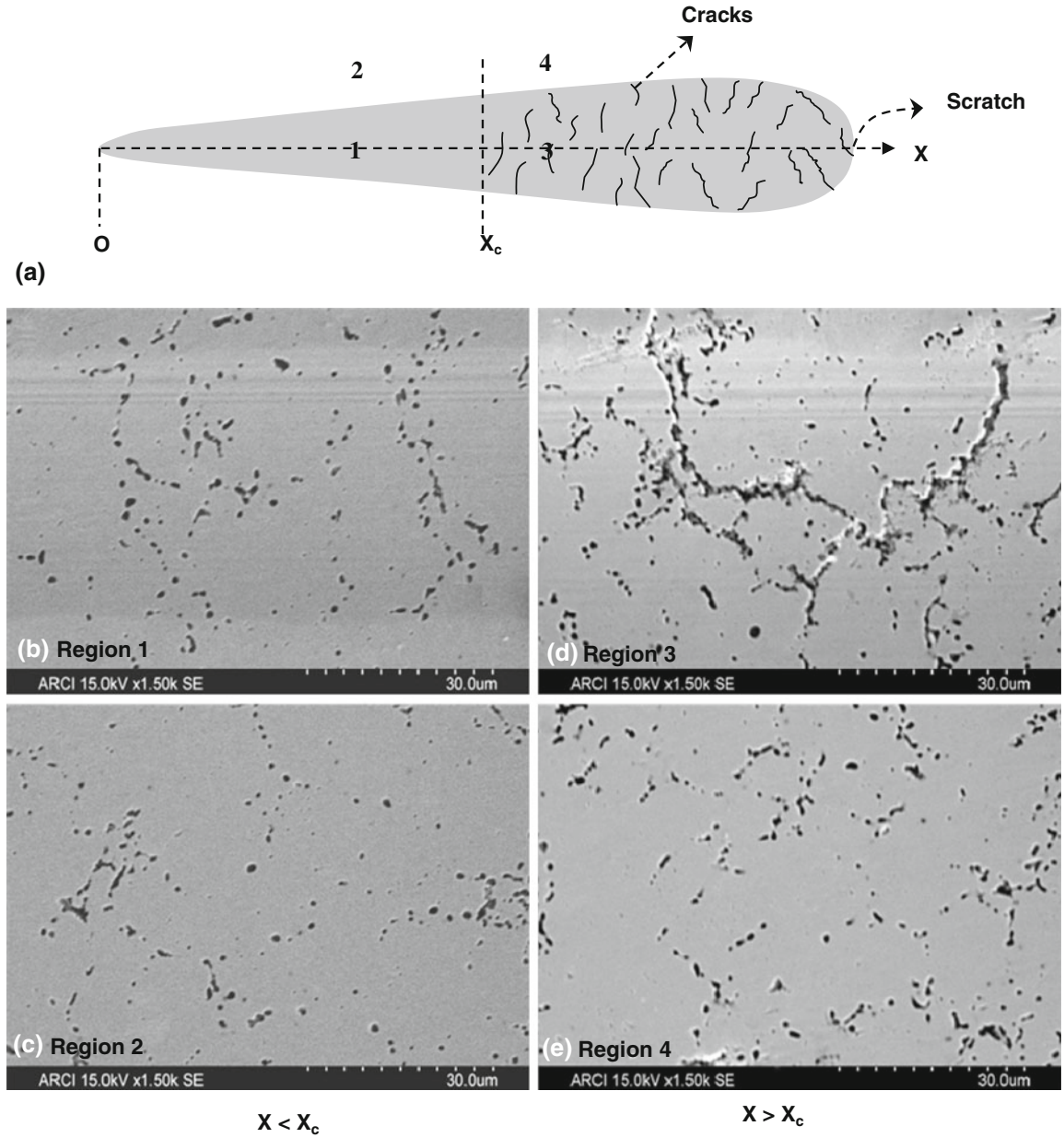

Fig. 2 (a) A schematic representation of the scratch defining the critical distance for cracking (X_c). (b) SEM micrograph of the scratch bottom at Region 1 ($X < X_c$) showing absence of cracks. (c) SEM micrograph of the scratch at Region 2 outside the scratch at $X < X_c$ showing absence of cracks. (d) SEM micrograph of the scratch bottom in Region 3 ($X > X_c$) showing the presence of cracks. (e) SEM micrograph of Region 4 outside the scratch ($X > X_c$) showing absence of cracks. (f) Low magnification view of scratch illustrating the transition from uncracked region to the cracked region with the marker X_c separating the two regions. (g) Higher magnification view of the region to the right of the marker X_c showing the presence of cracks at the scratch bottom. (h) Load-scratch length data from the scratch tester and the representation of L_c, the critical load for cracking

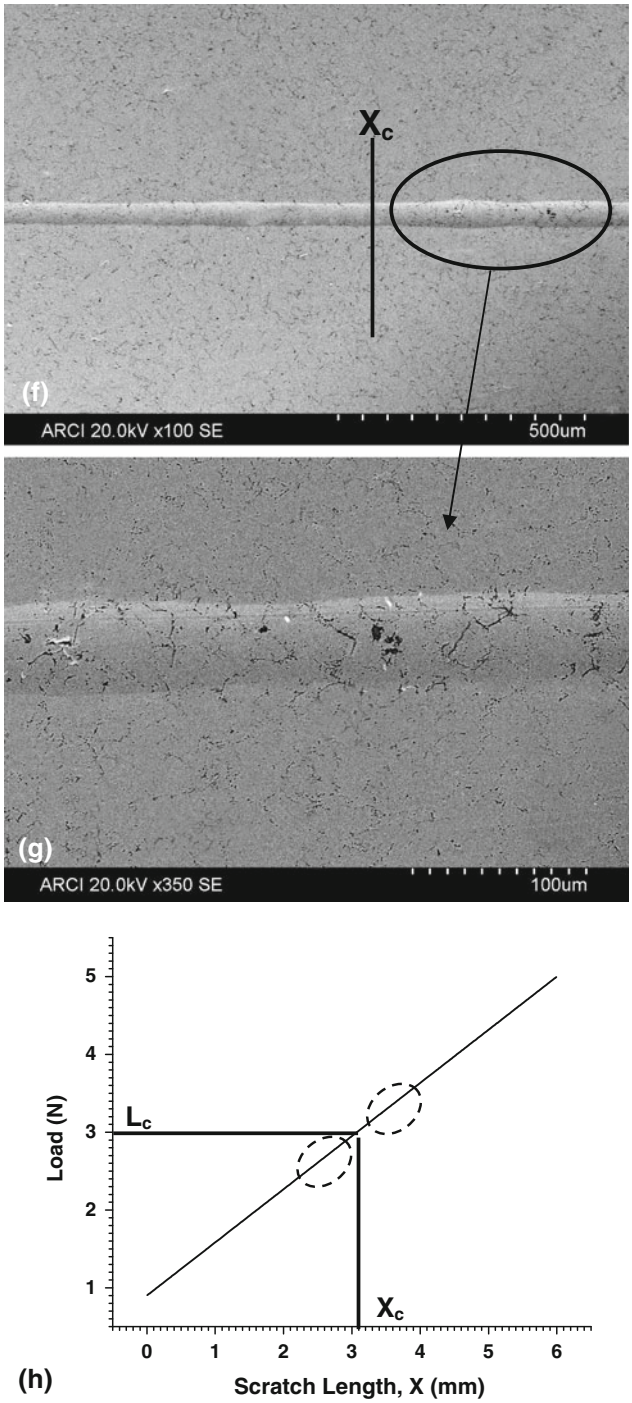

Fig. 2 continued

2.3 Influence of Porosity and Cracks on Elastic Modulus and Electrical Conductivity of Coatings

Considerable experimental and theoretical study on the influence of porosity and cracks (both inter-splat and vertical cracks) on the elastic modulus of air plasma spray coatings has been carried out (Ref 28-32). The effect of the pores and cracks on electrical conductivity of air plasma spray coatings, in contrast, has been less well studied (Ref 33-35). Theoretical and phenomenological models have been proposed to explain the dramatically lower elastic modulus and electrical conductivity exhibited by air plasma spray coatings compared to bulk material of identical composition. In general, many of these models lump the porosity, inter-splat cracks (unbonded regions), and also the vertical cracks found within the splats into a single parameter p which equals the cumulative volume fraction of all the above defects. Further, these models broadly show that while the ratio of the elastic modulus of the coating to that of the bulk (i.e., E_c/E_b; E_c = elastic modulus of the coating, and E_b = elastic modulus of the bulk material of identical composition as the coating) is proportional to the parameter $(1 - p)/(1 + ap)$ where a is a numerical constant approximately equal to 32 (Ref 30). In the case of electrical conductivity, the model at the simplest level reveals that the ratio of electrical conductivity of the coating to that of the bulk (i.e., σ_c/σ_b; σ_c = electrical conductivity of the coating, and σ_b is the electrical conductivity of bulk material of identical composition as the coating) is proportional to p itself (Ref 33).

If we now consider the extension of above results to cold spray coating, it is to be noted that the splats in cold spray coatings do not exhibit vertical cracks since the powder particles remain solid and transform to splats on impacting the substrate (or previously formed coating) purely by plastic deformation. Thus, solidification shrinkage-driven vertical cracks are absent in the cold-sprayed splats. In addition, the porosity levels in cold spray coatings are at least an order of magnitude lower than that of air plasma coatings. Though the magnitude of the porosity depends on the material being coated, the porosity levels are usually less than 0.5% as long as the material is coatable in terms of high deposition efficiency. As a result, the parameter p is dominated by the volume fraction of inter-splat cracks which oriented largely in the plane of the coating in the case of cold spray coatings. It follows then that the elastic modulus and electrical conductivity of cold-sprayed coatings are likely to be determined mainly by volume fraction of unbonded/not well-bonded inter-splat boundaries, and hence by the overall inter-splat bond strength of the cold spray coating. Incidentally, the critical load (L_c) for tensile cracking at the base of the scratch obtained using the scratch test is a direct measure of the inter-splat bond strength of the cold spray coating. Thus, it is to be expected that the parameters E_c, σ_c, and L_c of the coating shall be inter-related to each other and to the extent of bonding in the cold spray coating.

3. Results and Discussion

3.1 Microstructure and Porosity of the Coatings

Cold spray-coated samples were sectioned and polished and then etched. The etching process preferentially opened up the inter-splat boundaries which were weakly bonded or not at all bonded. The etched surface was then

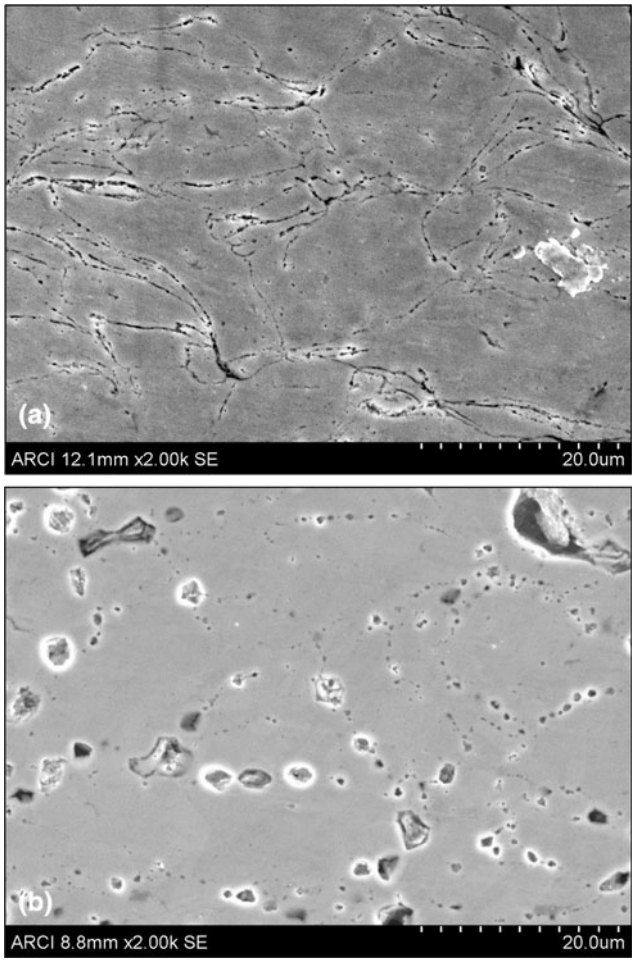

Fig. 3 SEM microstructure of cold-sprayed Cu coatings in the as-coated condition (a) and after heat treatment at 1073 K (b)

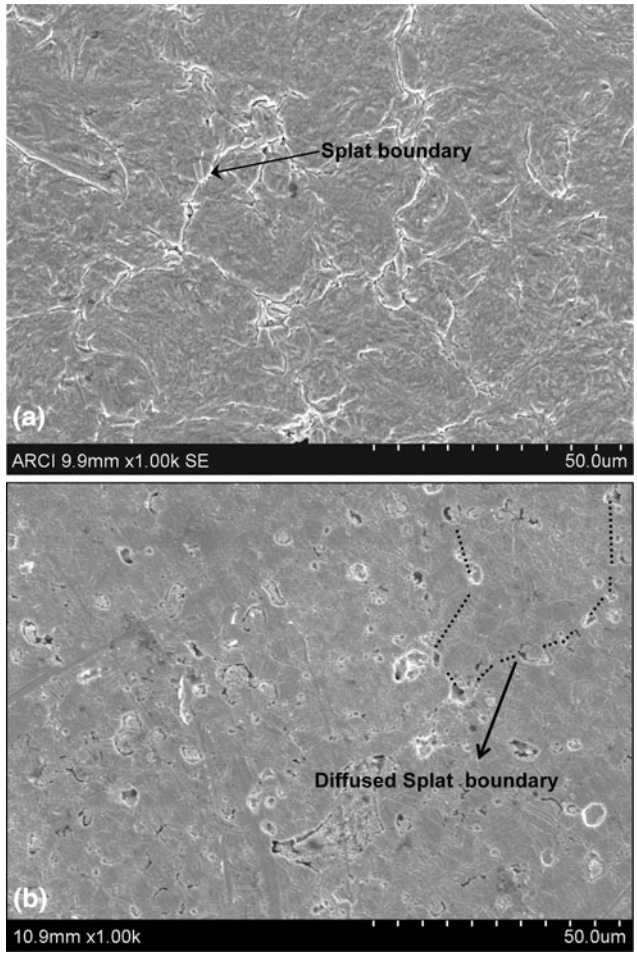

Fig. 4 SEM microstructure of cold-sprayed Ag coatings in the as-coated condition (a) and after heat treatment at 673 K (b)

examined in SEM to qualitatively estimate the extent of inter-splat bonding.

The SEM micrographs of the cold-sprayed Cu, Ag, Zn, and SS 316L coatings are presented in Fig. 3, 4, 5, and 6, respectively. In each of these figures, the micrographs of the coatings in the as-coated (Fig. 3a, 4a, 5a, 6a) and heat-treated conditions (Fig. 3b, 4b, 5b, 6b) are presented.

In the as-coated condition, all the coatings exhibit a substantial fraction of cracked (i.e., opened up by etching) inter-splat boundaries. Among the coatings, Ag coatings (Fig. 4a) exhibit the least proportion of cracked inter-splat boundaries in the as-coated condition, while Zn and SS 316L coatings (Fig. 5a and 6a, respectively) exhibit the highest proportion of cracked inter-splat boundaries. Cu coatings (Fig. 3a) exhibit intermediate proportion of cracked inter-splat boundaries.

The influence of heat treatment in reducing the density of cracked inter-splat boundaries is obvious in Cu, Ag, and SS 316L coatings. However, the effect is more dramatic in Cu and SS 316L coatings (Fig. 3b and 6b, respectively). In copper, heat treatment at 800 °C (Fig. 3b) eliminates the inter-splat cracks and leaves behind remnant pores/short cracks along the original cracked inter-splat boundaries. These pores/short cracks represent regions wherein the splats were too widely separated to be brought together by mass diffusion. The situation is similar in the case of SS 316L coatings since the heat treatment at 1100 °C has eliminated the inter-splat boundaries (Fig. 6b). However, the remnant cracks are longer and sharper in SS 316L coatings as compared to copper coatings. In Ag coating, the proportion and extent of inter-splat cracking is low even in the as-coated condition (see Fig. 4a) and thus, even though heat treatment reduces the extent of cracking (Fig. 4b), the effect is not dramatic.

Finally, in the case of Zn coating, heat treatment reduces the porosity (compare Fig. 5a and b), but the extent of inter-splat cracking is not reduced substantially by heat treatment (Fig. 5b). The behavior described above is unusual especially given the fact that the Zn coating was heat treated at a very high temperature (350 °C) equivalent to 90% of its melting point. A probable reason could be the fact that the water-atomized Zn powder used as the feed stock for cold spray coating was oxidized to a significant extent during the process of atomization. In order to check this postulate, XPS of the Zn powder feedstock was carried out, and the resulting spectra are presented

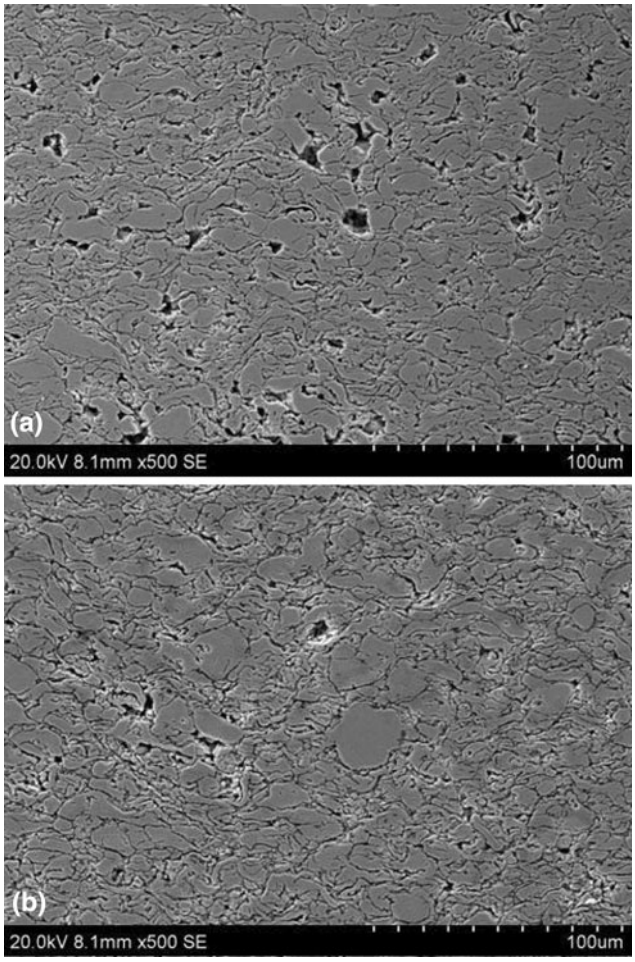

Fig. 5 SEM microstructure of cold-sprayed Zn coatings in the as-coated condition (a) and after heat treatment at 623 K (b)

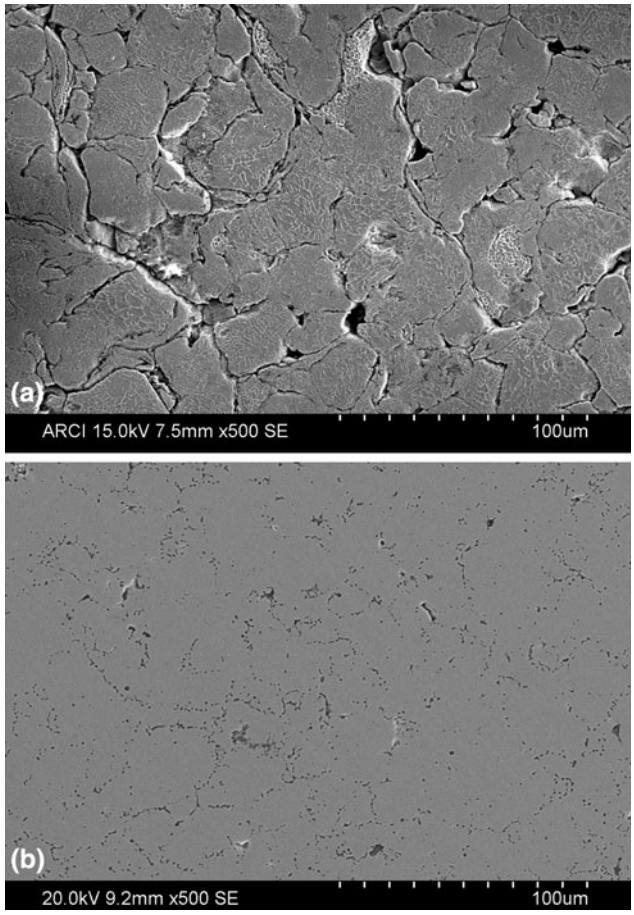

Fig. 6 SEM microstructure of cold-sprayed SS 316L coatings in the as-coated condition (a) and after heat treatment at 1373 K (b)

in Fig. 7(a). The XPS spectra clearly indicate the presence of significant amounts of oxygen on the Zn powder surface. In addition, a close examination of cold-mounted Zn powders using the SEM indicated the presence of gray regions (region marked as 2 in Fig. 7b) around the Zn particles (marked as 1 in Fig. 7b), and an EDAX scan of these two regions indicated a significant presence of oxygen in region 2 (Fig. 7c) and its complete absence in region 1 (Fig. 7d). Thus, region 2 represents the oxide scale present on the Zn powder surface.

The volume fraction of pores (not cracks) present in the coating were estimated in both the as-coated and heat-treated conditions, and the results are provided in Table 4. The variation of porosity with heat treatment temperature (T_{ht}) normalized by the melting point of the coating material (T_{mp}) is presented in Fig. 8. The melting point values used for computing T_{ht}/T_{mp} are presented in Table 1. In the case of coatings in the as-coated condition, heat treatment temperature is taken as room temperature (= 300 K). From Fig. 8, it is clear that among the four coatings, Ag and Cu coatings exhibit low porosity in the as-coated condition unlike 316 SS or Zn coatings. The above behavior is related to the fact that Cu and Ag particles are amenable to extensive plastic deformation on impacting the substrate due to their low hardness (see Table 4) and high ductility, and thus are able to fill the uneven coating surface quite well leading to low porosities. It is quite likely that the porosity levels in Cu and Ag coatings are underestimated since the pores and unbonded splat boundaries are filled up by plastically deformed metal during polishing. However, the trend of decreasing porosity with increasing heat treatment temperature (Fig. 8) is likely to remain valid. In the case of stainless steel powder particles, their high hardness (see Table 4) limits the extent of deformation during the cold spray process, and hence porosity is higher. The Zn powder particles are not amenable to extensive deformation not only due to their hcp structure but also due to the presence of oxide scale in these powders as pointed out earlier. As a result, in spite of its low melting point and hardness (see Table 1, 4), Zn coatings do exhibit higher porosity levels than Ag or Cu coatings. The decrease in porosity with increasing heat treatment temperature is related to the fact that some of the smaller pores are closed by mass diffusion. However, it should be noted that cracked inter-splat boundaries are more damaging than porosity in

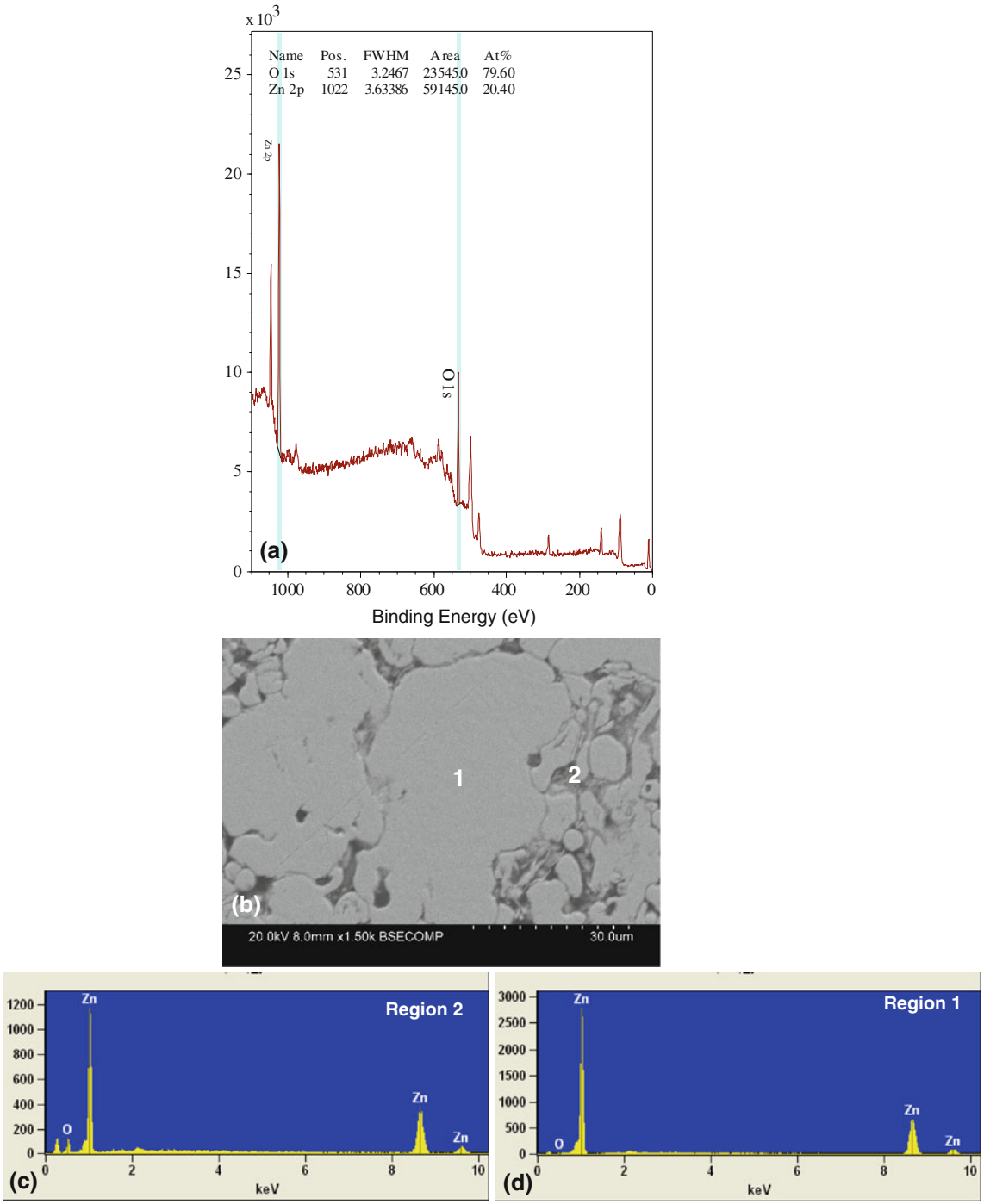

Fig. 7 (a) XPS spectra of the Zn feedstock. (b) SEM micrograph of cold-mounted Zn powders delineating regions 1 & 2. (c) The EDAX spectra from region 2. (d) The EDAX spectra from region 1

terms of their effects on elastic modulus and electrical conductivity of the coating.

3.2 Elastic Modulus, Electrical Conductivity, and Critical Load for Inter-Splat Debonding

The elastic modulus (E_c) and the electrical conductivity (σ_c) values of the four cold spray coatings as a function of heat treatment temperature are presented in Table 4. The variation of the elastic modulus of the cold spray coatings (E_c) normalized by the elastic modulus of bulk material of composition identical to that of the coating (E_b) is presented as a function of normalized heat treatment temperature (T_{ht}/T_{mp}) for all the four coatings in Fig. 9. The values of the elastic modulus (bulk) and the melting point used for computing E_c/E_b and T_{ht}/T_{mp} are provided in Table 1.

Table 4 Properties of the four cold spray coatings as a function of heat treatment

Coating	Heat treatment temp., K	Hardness, H_c, MPa	Elastic modulus, E_c, GPa	Porosity, %	Electrical conductivity, σ_c, MS/m	Critical load, L_c, N
Ag	300	1310	73.5	0.10	45.0	3.90
	673	850	74.6	0.06	47.3	4.56
	300	1661	82.7	0.20	19.2	1.12
Cu	673	1076	94.0	0.10	30.2	…
	873	920	99.4	0.08	33.4	…
	1073	713	115.0	0.07	36.5	4.37
Zn	300	573	62.4	0.47	5.51	1.71
	623	532	69.4	0.15	5.72	1.75
	300	2924	98.0	0.80	0.45	0.96
SS 316L	673	2604	123.0	0.76	…	…
	1073	2202	135.0	0.36	…	…
	1373	2114	164.0	0.20	0.80	3.01

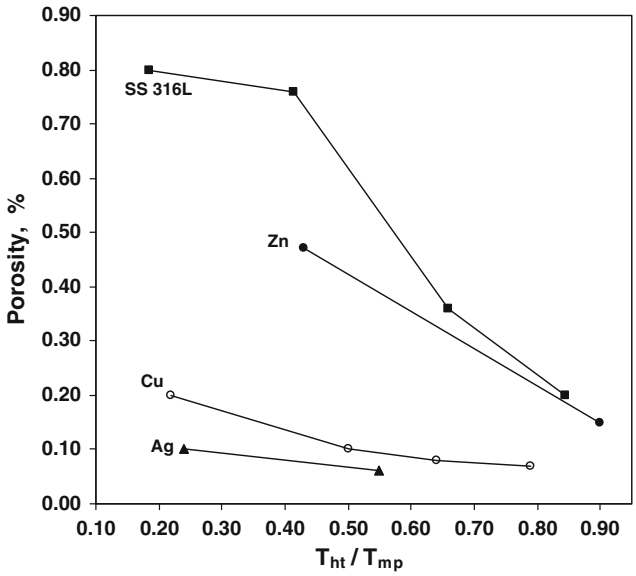

Fig. 8 The variation of porosity as a function of normalized heat treatment temperature (T_{ht}/T_{mp}) in the case of cold-sprayed Cu, Ag, Zn, and SS 316L coatings

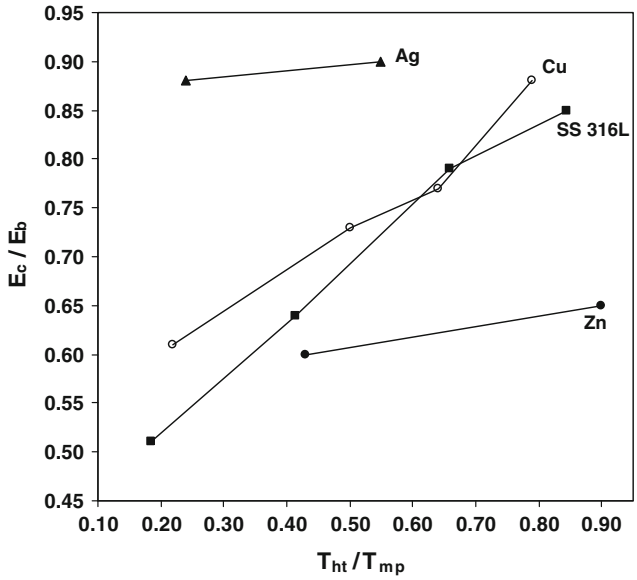

Fig. 9 The variation of normalized elastic modulus (E_c/E_b) as a function of normalized heat treatment temperature (T_{ht}/T_{mp}) in the case of cold-sprayed Cu, Ag, Zn, and SS 316L coatings

In all the four coatings, the ratio E_c/E_b increases with increasing heat treatment temperature reflecting the improvement in inter-splat bonding due to the diffusion process. Consistent with the fact that Ag coatings revealed the lowest density of inter-splat cracks (see Fig. 4), they exhibit the highest E_c/E_b values around 0.9 (i.e., coating modulus is 90% of bulk elastic modulus of Ag). SS 316L coatings in the as-coated condition exhibit the highest inter-splat crack density (see Fig. 6a), and thus had the lowest E_c/E_b values among the four coatings (around 0.5). However, with increasing heat treatment temperature, the value of E_c/E_b of SS 316L coating increases substantially due to improved inter-splat bonding (see Fig. 6, 9). Cu coating exhibits a behavior similar to that of SS 316L coating. In the case of Zn coating, consistent with the observation that inter-splat crack density decreased only marginally with heat treatment due to the presence of oxide scale on the surface of the powder, the E_c/E_b values also increased only marginally upon heat treatment.

In Fig. 10, the variation of normalized electrical conductivity with T_{ht}/T_{mp} is presented for all the four cold spray coatings. The results are very similar to that of Fig. 9, and thus the observations and explanations provided earlier in respect of elastic modulus of the coatings are equally valid for electrical conductivity of the coatings. In particular, it may be noted that the electrical conductivity values of Zn coatings are particularly low, and this can be attributed to the presence of remnant oxide scale in the inter-splat boundaries caused by pinching out of the oxides on the Zn powder surfaces (see Fig. 7b).

The values of L_c obtained in the case of all the four cold spray coatings, either in the as-coated condition or heat treated at the highest temperature, are presented in Table 4. The variation of L_c with the normalized

heat-treatment temperature (T_{ht}/T_{mp}) is presented in Fig. 11. Once again, the trends are very similar to the variation of E_c/E_b and σ_c/σ_b with T_{ht}/T_{mp}. L_c increases with increasing T_{ht}/T_{mp} in all the coatings. The L_c values are the highest for Ag coating and the lowest for Zn coating and in both these coatings, L_c increases marginally with increasing heat treatment temperature, however, for different reasons as stated earlier. In the case of Cu and SS 316L coatings, on the other hand, L_c increases dramatically with increasing heat treatment temperature.

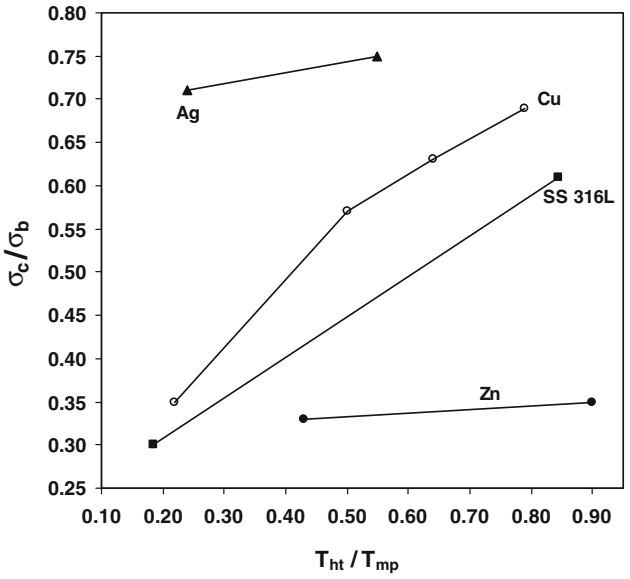

Fig. 10 The variation of normalized electrical conductivity of (σ_c/σ_b) of cold-sprayed Zn, SS 316L, Cu, and Ag coatings as a function of heat treatment temperature (T_{ht}/T_{mp})

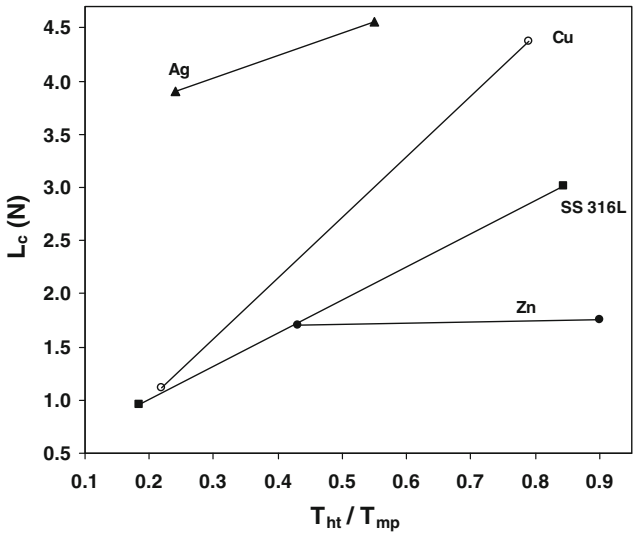

Fig. 11 The variation of critical load for inter-splat debonding (L_c) as a function of normalized heat treatment temperature (T_{ht}/T_{mp}) in the case of cold-sprayed Zn, SS 316L, Cu, and Ag coatings

3.3 Concluding Remarks

On the basis of the results presented in Sect 3.2 and 3.3, it can be concluded that the normalized elastic modulus (E_c/E_b), normalized electrical conductivity (σ_c/σ_b), and critical load (L_c) of the cold spray coatings correlate very well with the extent of inter-splat bonding as determined by microscopical examination of the coatings (Sect 3.1). It then follows that the parameters E_c/E_b, σ_c/σ_b, and L_c are inter-related to each other. Figures 12 to 14 indicate that such is the case. For example, in Fig. 12, an increase in σ_c/σ_b of the cold spray coating causes a corresponding increase in E_c/E_b. However, at higher values of σ_c/σ_b, the E_c/E_b increases, but only marginally. This suggests that σ_c/σ_b is more sensitive to the extent of inter-splat bonding than E_c/E_b especially when the cold spray coating is denser with fewer poorly bonded inter-splat boundaries. Similarly, from Fig. 13 wherein E_c/E_b is plotted against L_c, it is clear that L_c is more sensitive to the extent of inter-splat bonding than E_c/E_b. In contrast, the relationship between σ_c/σ_b and L_c is nearly linear (Fig. 14) indicating that both these parameters are equally and strongly sensitive to the extent of inter-splat bonding in the cold spray coating over the whole range from low level to high level of inter-splat bonding.

Thus, it can be concluded that the electrical conductivity and the critical load obtained from scratch testing are better parameters for evaluating the extent of inter-splat bonding in the cold spray coatings. Of these, electrical conductivity test is easier to carry out and is also a non-destructive test. However, it may not be a good technique in the case of coatings with low conductivity. In such cases, scratch testing to obtain L_c may be a better technique to evaluate the extent of inter-splat bonding in cold spray coatings.

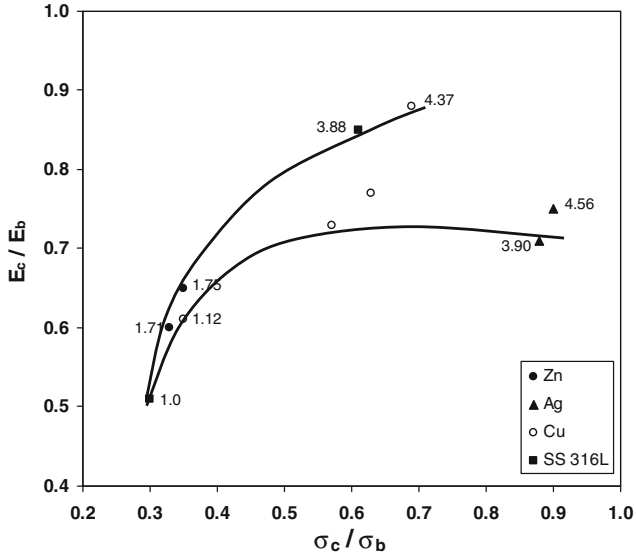

Fig. 12 The correlation between the normalized elastic modulus and normalized electrical conductivity in the case of the four cold spray coatings

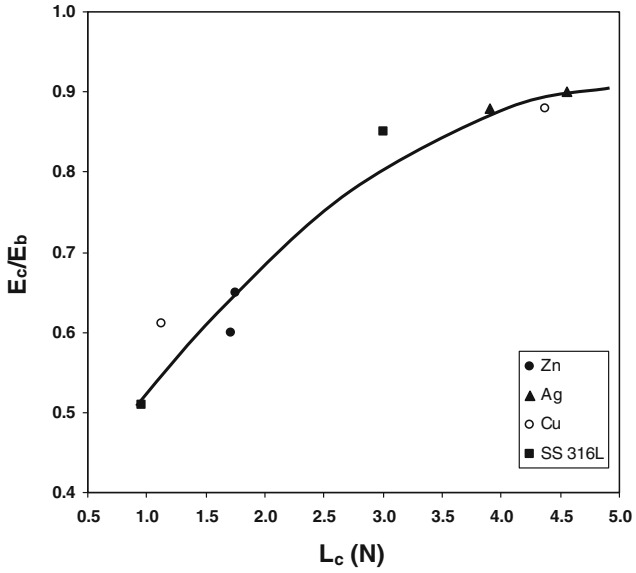

Fig. 13 The correlation between the normalized elastic modulus (E_c/E_b) and the critical load (L_c) for inter-splat debonding in the case of the four cold spray coatings

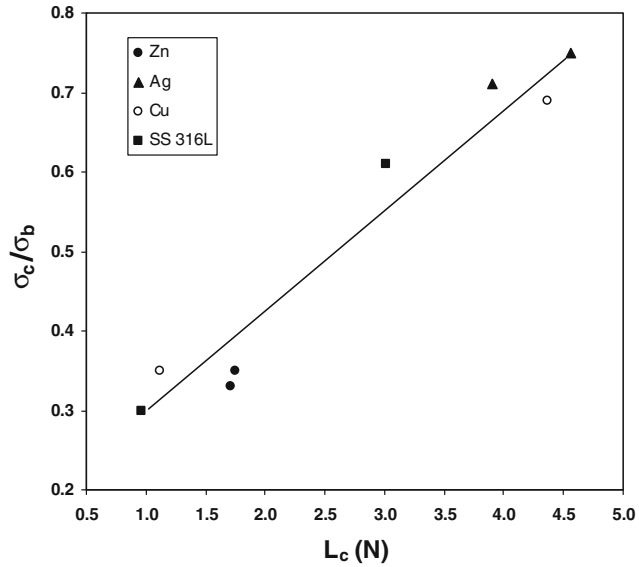

Fig. 14 The correlation between the normalized electrical conductivity (σ_c/σ_b) and the critical load (L_c) for inter-splat debonding in the case of the four cold spray coatings

This study has shown that electrical conductivity and critical load for cracking are excellent techniques to estimate the extent and strength of inter-splat bonding. However, the inter-splat bond strength ultimately determines the performance of the coating, and thus there is a clear need to establish the correlation between the electrical conductivity and critical load of the cold spray coatings with their performance (e.g., tribological behavior, corrosion behavior) before these indirect techniques can serve as quality control techniques.

4. Conclusions

This article represents a preliminary attempt to quantify the extent of inter-splat bonding in cold spray coatings utilizing indirect parameters like elastic modulus, electrical conductivity, and critical load for inter-splat debonding. Results obtained in this study indicate that electrical conductivity and critical load for inter-splat debonding are appropriate parameters capable of quantifying the extent of inter-splat bonding over the whole range from low to high proportion of inter-splat bonding and thus can serve as good indicators of cold spray coating quality.

References

1. W.-Y. Li, C.-J. Li, and H. Liao, Effect of Annealing Treatment on the Microstructure and Properties of Cold Sprayed Copper Coating, *J. Therm. Spray Technol.*, 2006, **15**, p 206-211
2. P. Sudharshan Phani, D. Srinivasa Rao, S.V. Joshi, and G. Sundararajan, Effect of Process Parameters and Heat Treatments on Properties of Cold Sprayed Copper Coatings, *J. Therm. Spray Technol.*, 2007, **16**, p 425-434
3. P. Sudharshan Phani, V. Vishnukanthan, and G. Sundararajan, Effect of Heat Treatment on Properties of Cold Sprayed Nanocrystalline Copper Alumina Coatings, *Acta Mater.*, 2007, **55**, p 4741-4751
4. R.C. McCune, W.T. Donion, O.O. Popoola, and E.L. Cartwright, Characterization of Copper Layers Produced by Cold Gas Dynamic Spraying, *J. Therm. Spray Technol.*, 2000, **9**(1), p 73-82
5. T. Novoselova, P. Fox, R. Morgan, and W. O'Neill, Experimental Study of Titanium/Aluminium Deposits Produced by Cold Gas Dynamic Spray, *Surf. Coat. Technol.*, 2006, **200**, p 2775-2783
6. H.-R. Wang, W.-Y. Li, L. Ma, J. Wang, and Q. Wang, Corrosion Behavior of Cold Sprayed Titanium Protective Coating on 1Cr13 Substrate in Seawater, *Surf. Coat. Technol.*, 2007, **201**, p 5203-5206
7. C.-J. Li and W.-Y. Li, Deposition Characteristics of Titanium Coating in Cold Spraying, *Surf. Coat. Technol.*, 2003, **167**, p 278-283
8. L. Ajdelsztajn, B. Jodoin, and J.M. Schoenung, Synthesis and Mechanical Properties of Nanocrystalline Ni Coatings Produced by Cold Gas Dynamic Spraying, *Surf. Coat. Technol.*, 2006, **201**, p 1166-1172
9. T. Van Steenkiste and D.W. Gorkiewicz, Analysis of Tantalum Coatings Produced by the Kinetic Spray Process, *J. Therm. Spray Technol.*, 2003, **13**(2), p 265-273
10. N. Bala, H. Singh, and S. Prakash, High-Temperature Oxidation Studies of Cold-Sprayed Ni-20Cr and Ni-50Cr Coatings on SAE 213-T22 Boiler Steel, *Appl. Surf. Sci.*, 2009, **255**, p 6862-6869
11. H.Y. Lee, S.H. Jung, S.Y. Lee, and K.H. Ko, Alloying of Cold-Sprayed Al-Ni Composite Coatings by Post-Annealing, *Appl. Surf. Sci.*, 2007, **253**, p 3496-3502
12. W.-Y. Li, C. Zhang, H. Liao, J. Li, and C. Coddet, Characterization of Cold-Sprayed Nickel-Alumina Composite Coating with Relatively Large Nickel-Coated Alumina Powder, *Surf. Coat. Technol.*, 2008, **202**, p 4855-4860
13. X. Guo, G. Zhang, W.Y. Li, L. Dembinski, Y. Gao, H. Liao, and C. Coddet, Microstructure, Microhardness and Dry Friction Behavior of Cold-Sprayed tin Bronze Coatings, *Appl. Surf. Sci.*, 2007, **254**, p 1482-1488
14. G. Sundararajan, P. Sudharshan Phani, A. Jyothirmayi, and R.C. Gundakaram, The Influence of Heat Treatment on the Microstructural, Mechanical and Corrosion Behaviour of Cold Sprayed SS 316L Coatings, *J. Mater. Sci.*, 2009, **44**, p 2320-2326
15. W.-Y. Li, H. Liao, G. Douchy, and C. Coddet, Optimal Design of a Cold Spray Nozzle by Numerical Analysis of Particle Velocity and Experimental Validation with 316L Stainless Steel Powder, *Mater. Des.*, 2007, **28**, p 2129-2137

16. P. Richer, A. Zúñiga, M. Yandouzi, and B. Jodoin, CoNiCrAlY Microstructural Changes Induced During Cold Gas Dynamic Spraying, *Surf. Coat. Technol.*, 2008, **203**, p 364-371
17. H.-T. Wang, C.-J. Li, G.-J. Yang, and C.-X. Li, Effect of Heat Treatment on the Microstructure and Property of Cold-Sprayed Nanostructured $FeAl/Al_2O_3$ Intermetallic Composite Coating, *Vacuum*, 2009, **83**, p 146-152
18. F. Gartner, C. Borchers, T. Stoltenhoff, and H. Kreye, Numerical and Microstructural Investigations of Bonding Mechanisms in Cold Spraying, *Thermal Spray 2003: Advancing the Science and Applying the Technology*, C. Moreau and B. Marple, Ed., ASM International, Materials Park, Ohio, 2003, p 1-7
19. H. Assadi and F. Gartner, Thorsten Stoltenhoff and Heinrich Kreye, Bonding Mechanism in Cold Gas Spraying, *Acta Mater.*, 2003, **51**, p 4379-4394
20. M. Grujicic, J.R. Saylora, D.E. Beasleya, W.S. DeRossetb, and D. Helfritch, Computational Analysis of the Interfacial Bonding Between Feed-Powder Particles and the Substrate in the Cold-Gas Dynamic-Spray Process, *Appl. Surf. Sci.*, 2003, **219**, p 211-227
21. M. Grujicic, C.L. Zhao, W.S. DeRosset, and D. Helfritch, Adiabatic Shear Instability Based Mechanism for Particles/Substrate Bonding in the Cold-Gas Dynamic-Spray Process, *Mater. Des.*, 2004, **25**, p 681-688
22. W.-Y. Li, C. Zhang, X. Guo, C.-J. Li, H. Liao, and C. Coddet, Study on Impact Fusion at Particle Interfaces and Its Effect on Coating Microstructure in Cold Spraying, *Appl. Surf. Sci.*, 2007, **254**, p 517-526
23. D. Zhang, P.H. Shipway, and D.G. McCartney, Particle Substrate Interactions in Cold Gas Dynamic Spraying, *Thermal Spray 2003: Advancing the Science and Applying the Technology*, C. Moreau and B. Marple, Ed., ASM International, Materials Park, Ohio, 2003, p 45-52
24. A.N. Papyrin, S.V. Klinkov, and V.F.Kosarev, Modelling of Particle Substrate Adhesive Interactions Under Cold Spray Process, *Thermal Spray 2003: Advancing the Science and Applying the Technology*, C. Moreau and B. Marple, Ed., ASM International, Materials Park, Ohio, 2003, p 27-35
25. S.J. Bull and E.G. Berasetegui, An Overview of the Potential of Quantitative Coating Adhesion Measurement by Scratch Testing, *Tribol. Int.*, 2006, **39**, p 99-114
26. N.M. Chavan and G. Sundararajan, International Advanced Research Centre for Powder Metallurgy and New Materials, Hyderabad, India, 2009, unpublished work
27. W.C. Oliver and G.M. Pharr, An Improved Technique for Determining Hardness and Elastic Modulus Using Load and Displacement Sensing Indentation Experiments, *J. Mater. Res.*, 1992, **7**(6), p 1564-1583
28. J. Luo and R. Stevens, Porosity-Dependence of Elastic Moduli and Hardness of 3Y-TZP Ceramics, *Ceram. Int.*, 1999, **25**, p 281-286
29. T. Nakamura, G. Qian, and C. Berndt, Effects of Pores on Mechanical Properties of Plasma-Spray Ceramic Coatings, *J. Am. Ceram. Soc.*, 2000, **83**(3), p 578-584
30. F. Azarmi, T. Coyle, and J. Mostaghimi, Young's Modulus Measurement and Study of the Relationship Between Mechanical Properties and Microstructure of Air Plasma Sprayed Alloy 625, *Surf. Coat. Technol.*, 2009, **23**, p 1045-1054
31. I. Sevostianov and M. Kachanov, Modelling of the Anisotropic Elastic Properties of Plasma-Sprayed Coatings in Relation to Their Microstructure, *Acta Mater.*, 2000, **48**, p 1361-1370
32. M. Landa, F. Kroupa, K. Neufuss, and P. Urbanek, Effect of Uniaxial Pressure on Ultrasound Velocities and Elastic Moduli in Plasma-Sprayed Ceramics, *J. Therm. Spray Technol.*, 2003, **12**(2), p 226-233
33. R. McPherson, A Model for the Thermal Conductivity of Plasma-Sprayed Ceramic Coatings, *Thin Solid Films*, 1984, **112**, p 89-95
34. S. Boire-Lavigne, C. Moreau, and R.G. Saint-Jacques, The Relationship Between the Microstructure and Thermal Diffusivity of Plasma-Sprayed Tungsten Coatings, *J. Therm. Spray Technol.*, 1995, **4**(3), p 261-267
35. I. Sevostianov and M. Kachanov, Plasma-Sprayed Ceramic Coatings: Anisotropic Elastic and Conductive Properties in Relation to the Microstructure, Cross-Property Correlation, *Mater. Sci. Eng. A*, 2001, **297**, p 235-243
36. F. Cardarelli, *Materials Hand Book*, 2nd ed., Springer, 1999, p 101-123, 179-186, 187-196, 393-400